ACI STRUCTURAL JOURNAL TECHNICAL PAPER

Title No. 114-S03

Hysteresis Modeling of Reinforced Concrete Structures: State of the Art

by Piyali Sengupta and Bing Li

Hysteresis modeling of reinforced concrete (RC) structures requires a constitutive relationship capable of producing requisite strength and stiffness degradation and pinching at all displacement levels. Moreover, the hysteresis model must be generic, computationally efficient, and mathematically tractable so as to perform satisfactorily with random input functions. Thus, development of hysteresis models with the entire prerequisites may become stringent considering the numerous parameters contributing to the structural behavior. Hence, an extensive literature review is conducted to comprehend the hysteresis models of RC structures developed by various researchers. Then, a comprehensive synopsis of the state of the art along with the substantive findings is reported in the present paper. Thereafter, a comparative study between the existing hysteresis models and the experimental results of RC structural components under quasi-static cyclic loading is conducted to evaluate the performance of the hysteresis models.

Keywords: analytical modeling; degradation; hysteresis; pinching; reinforced concrete.

INTRODUCTION

The devastating consequences of the natural and man-made hazards across the globe in terms of the human casualties and the huge economic loss due to massive structural damage are well documented in the past few decades. With growth of urbanization, more people and properties become potential targets of the impending hazards in urban and metropolitan areas. Consequently, performance assessment of reinforced concrete (RC) structures has gained immense popularity among researchers and engineers. Thus, for performance evaluation of RC structures under repeated cyclic loading, prediction of the structural hysteresis behavior is of utmost significance.

A hysteresis model is capable of producing a load-deformation relationship of a structural member under repeated cyclic loading. The hysteresis models can be broadly classified into polygonal hysteresis models (PHMs) and smooth hysteresis models (SHMs). In polygonal hysteresis models, stiffness changes are considered at cracking, yielding, strength, and stiffness degradation stages. In SHMs, continuous stiffness changes due to yielding and sharp changes during unloading and deteriorating are considered. This paper documents the primary characteristics and limitations of the hysteresis models reported in the existing literature. Thereafter, a comparative study between the existing hysteresis models and the experimental results of RC structural components is presented to assess the performance of the hysteresis models.

RESEARCH SIGNIFICANCE

Hysteresis modeling of reinforced concrete (RC) structural components is a pertinent stage in performance assessment of structures under extreme loading conditions. Hence, the primary objective of this research is to accumulate and comprehend the existing hysteresis models developed by various researchers so as to evaluate and compare their performances with respect to the past experimental results of RC structural components. The substantive findings of this research are conveyed herein so that this study can be useful to engineers and researchers for the development of new hysteresis models with further accuracy and computational efficiency in the future.

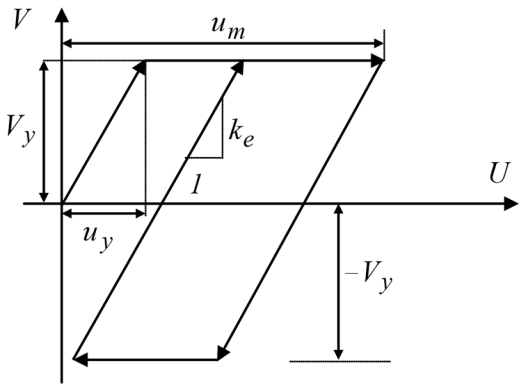

Fig. 1—Load-deflection diagram of elasto-plastic model.[1]

REVIEW OF EXISTING HYSTERESIS MODELS

The basic requirement of hysteresis models of reinforced concrete (RC) structures is the capability of producing requisite degradation and pinching at all displacement levels. Extensive research has been undertaken by various researchers to characterize hysteresis behavior of RC structural components. A brief review on the selective hysteresis models are presented in this section.

Polygonal hysteresis model

The elasto-plastic model by Veletsos et al.,[1] as shown in Fig. 1, is represented by an elastic curve indicating the cracked section behavior with no incremental stiffness upon yielding. The variables V_y, u_y, and k_e are the yield strength, yield displacement, and elastic stiffness, respectively.

The bilinear degrading stiffness model by Clough et al.[2] operates on a bilinear primary curve with ascending post-

ACI Structural Journal, V. 114, No. 1, January-February 2017.
MS No. S-2015-141.R2, doi: 10.14359/51689422, received February 8, 2016, and reviewed under Institute publication policies.

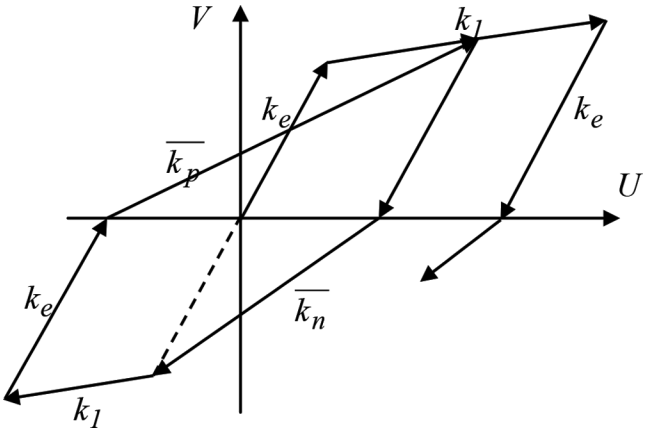

Fig. 2—Load-deflection diagram of bilinear degrading stiffness model.[2]

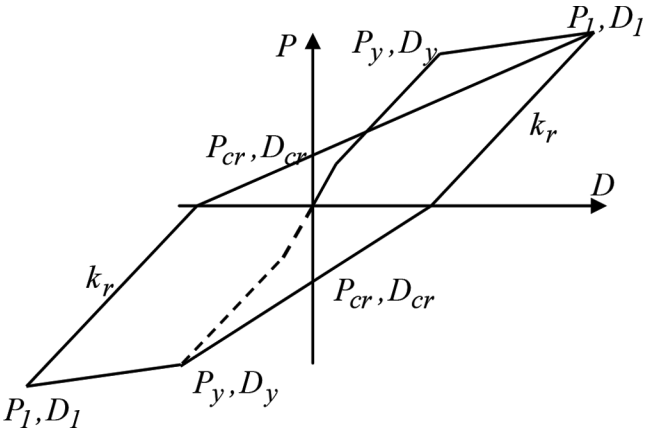

Fig. 3—Load-deflection diagram of trilinear degrading stiffness model.[3]

yielding branches and stiffness degradation at load reversals, as shown in Fig. 2. The post-yielding stiffness k_1 is defined as $k_1 = rk_e$, where k_e is elastic stiffness and r is the stiffness ratio. Here, the reloading branch projects toward the previous unloading point of the loading history.

The trilinear primary curve of the Takeda model[3] represents the uncracked, cracked, and post-yielding stages, as shown in Fig. 3. The unloading stiffness k_r is calculated in terms of yielding stiffness k_y, yield deflection D_y, and maximum deflection D_{max} as follows. In this model, the reloading branch projects toward the previous unloading point of the loading history.

$$k_r = k_y(D_y/D_{max})^{0.4} \quad (1)$$

In peak-oriented degrading bilinear (DBL) model by Imbeault and Nielsen,[4] as shown in Fig. 4, stiffness K changes from primary stiffness K_0 when the prior maximum deformation is exceeded.

$$K = K_0(D_y/D_{max})^{\alpha} \quad (2)$$

where D_y is yield deformation; D_{max} is maximum deformation in any direction; and α is a constant.

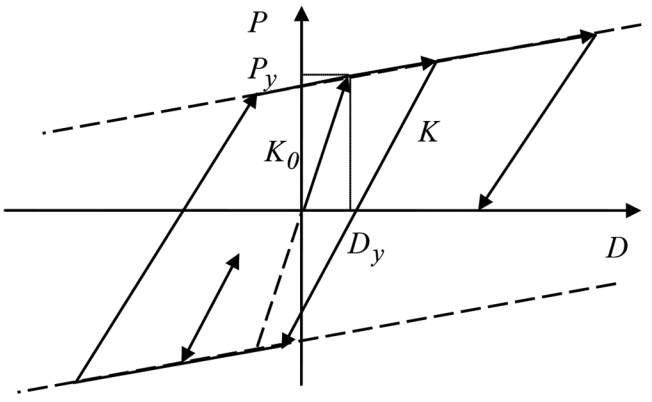

Fig. 4—Load-deflection diagram of degrading bilinear model.[4]

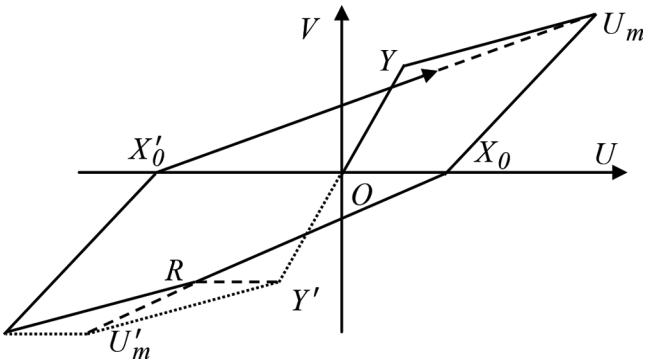

Fig. 5—Load-deflection diagram of Q-hysteresis model.[5]

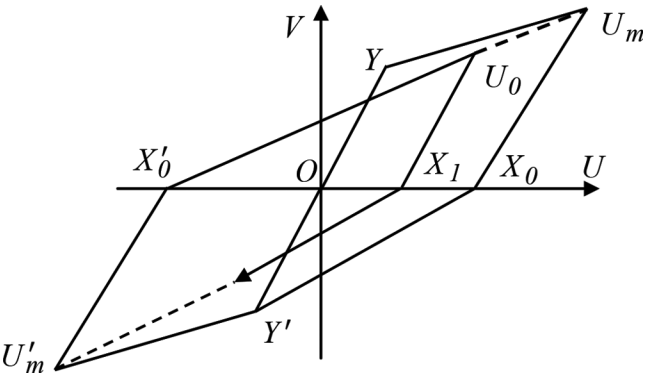

Fig. 6—Load-deflection diagram of hysteresis model.[6]

In the bilinear primary curve of Q-hysteresis model by Saidi and Sozen,[5] as shown in Fig. 5, unloading stiffness k_q in terms of elastic stiffness k, yield deformation U_y, maximum deformation U_m, and constant α is shown in the following expression. Reloading stiffness is determined as slope of the line X_0U_m', with U_m' being the point on the primary curve symmetric to U_m with respect to origin.

$$k_q = k(U_y/U_m)^{\alpha} \quad (3)$$

The bilinear primary curve of the hysteresis model developed by Otani[6] is shown in Fig. 6. The expression for unloading slope S_1 in terms of the elastic slope S_{OY}, yield displacement U_y, maximum displacement U_m and empirical constant α is mentioned as follows.

$$S_1 = S_{OY}(U_y/U_m)^{\alpha} \quad (4)$$

The hysteresis shear model by Ozcebe and Saatcioglu[7] shown in Fig. 7 was derived based on statistical analysis of experimental data. Unloading slope k from a load between cracking load V_{cr} and yield load V_y is defined in terms of cracking stiffness k_1, cracking deflection Δ_{cr}, yield deflection Δ_y, unloading deflection Δ, and slope of the line joining cracking and yield points k_2.

$$k = k_1 - \frac{k_1 - k_2}{\Delta_y - \Delta_{cr}}(\Delta - \Delta_{cr}) \quad (5)$$

When V_y is exceeded, unloading from loads above and below V_{cr} follows slopes k, respectively.

$$k = k_2\left\langle 1 - 0.05\frac{\Delta}{\Delta_y}\right\rangle \quad (6)$$

$$k = 0.6k_2\left\langle 1 - 0.07\frac{\Delta}{\Delta_y}\right\rangle \quad (7)$$

Reloading follows the primary curve until a load higher than V_{cr} is reversed. When V_{cr} is exceeded, reloading until V_{cr} and beyond V_{cr} follow lines passing through points (Δ_p, V_p') and (Δ_m, V_m'), respectively, up to primary curve, and post intersection, the reloading branch follows the primary curve.

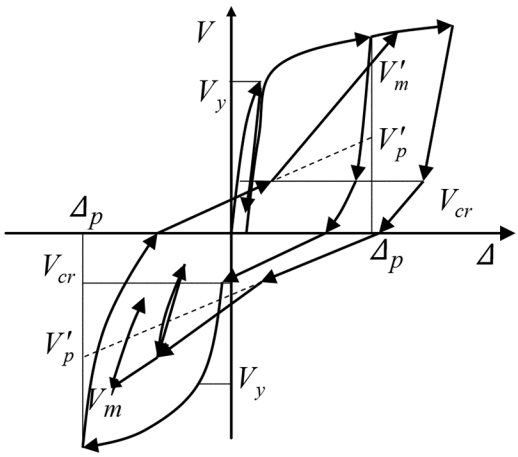

Fig. 7—Load-deflection diagram of hysteresis shear model.[7]

$$V_p' = V_p e^{\alpha}(\Delta_p/\Delta_y) \quad (8)$$

$$\alpha = 0.82(N/N_0) - 0.14 < 0.0 \quad (9)$$

$$V_m' = V_m e[\beta n + \gamma(\Delta_m/\Delta_y)] \quad (10)$$

$$\beta = -0.014\sqrt{\Delta_m/\Delta_y} \quad (11)$$

$$\gamma = -0.010\sqrt{n} \quad (12)$$

where N is the axial compressive force; N_0 is nominal axial load capacity; n is a counter tracing number of cycles at constant displacement; and α, β, and γ are mathematical coefficients.

In pivot hysteresis model by Dowell et al.,[8] quadrants Q_1, Q_2, Q_3, and Q_4 of the monotonically increasing loading envelope defined by the horizontal axis and elastic loading lines represent elastic stiffness, strain-hardening stiffness, strength degradation, and residual strength (as displayed in Fig. 8). The primary pivot points (P_1, P_4) and pinching pivot points (PP_2, PP_4), as shown in Fig. 9, define softening and pinching (β_i), respectively. Positions of pinching pivot points change when maximum displacement $d_{i\,max}$ is more than strength degradation displacement d_{ti}.

$$\beta_i^* = \frac{F_{i\,max}}{F_{ti}}\beta_i \quad (13)$$

where $F_{i\,max}$ and F_{ti} are the maximum and strength degradation loads, respectively.

The energy-based hysteresis model by Sucuoglu and Erberik[9] for deteriorating systems operates on a bilinear curve with elastic stiffness K_0, post-yielding stiffness αK_0; unloading stiffness K_u, and reloading stiffness K_r, as shown in Fig. 10. To relate the loss in energy dissipation capacity in the displacement cycle with the reduced strength, a deteriorating system with yield strength F_y and yield displacement u_y and subjected to displacement U_m, as shown in Fig 11, is used. The energy dissipated in first cycle, $E_{h,1}$ and n-th cycle

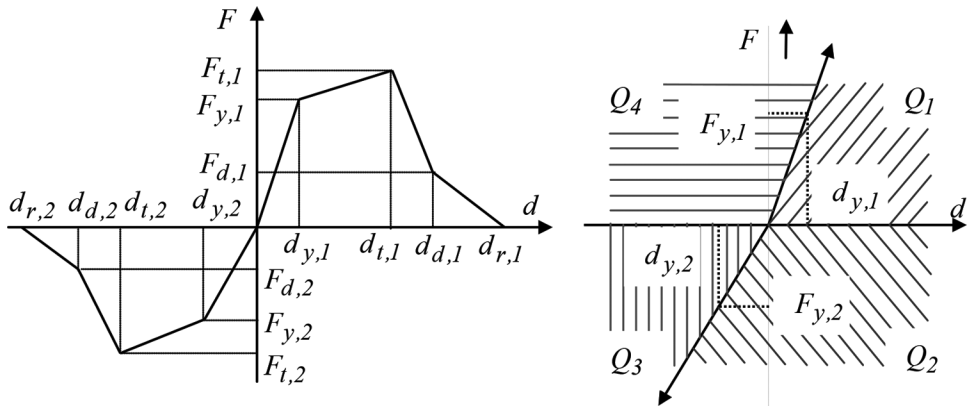

Fig. 8—Strength envelope and quadrant definition in pivot hysteresis model.[8]

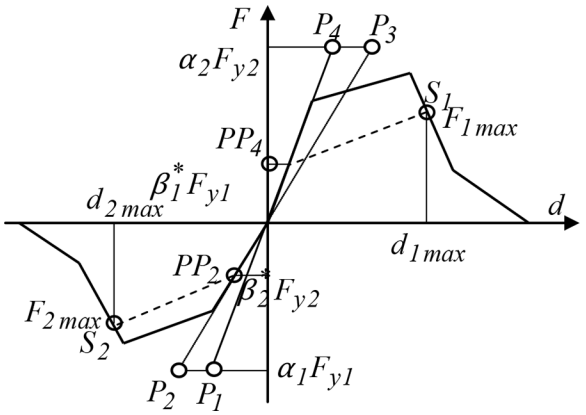

Fig. 9—Pivot point designation in pivot hysteresis model.[8]

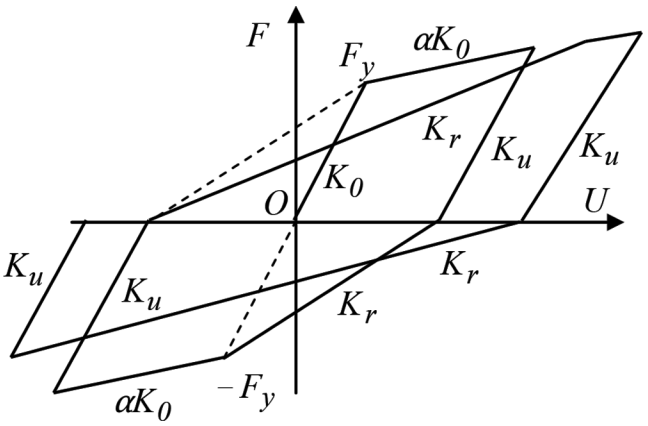

Fig. 10—Load-deflection diagram of energy-based hysteresis model.[9]

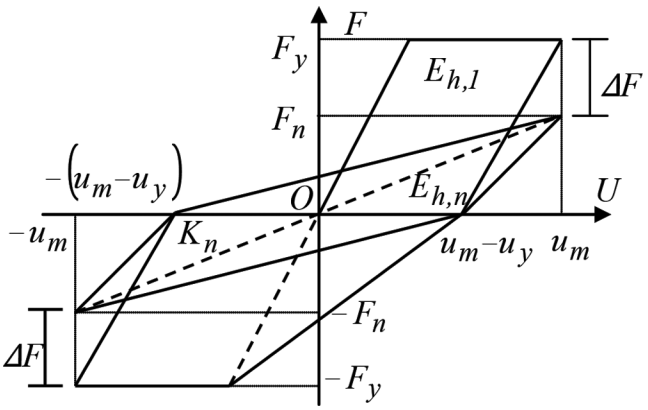

Fig. 11—Relationship between reduced strength and dissipated energy of energy-based hysteresis model.[9]

$E_{h,n}$ in terms of associated reduced strength at n-th cycle F_n are

$$E_{h,1} = 2.5F_y(u_m - u_y) \quad (14)$$

$$E_{h,n} = 2.5F_n(u_m - u_y) \quad (15)$$

$$E_{h,n}/E_{h,1} = 0.8(F_n/F_y) \quad (16)$$

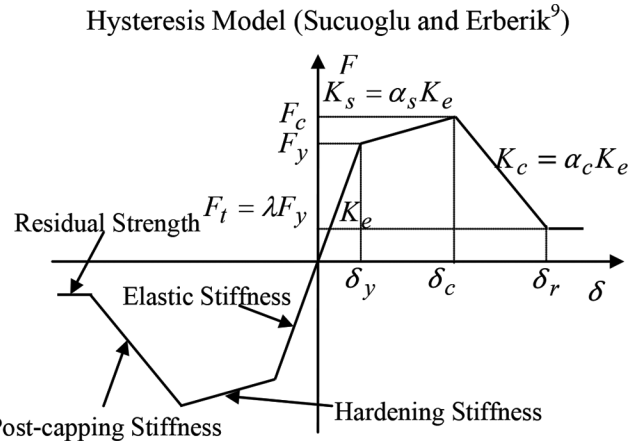

Fig. 12—Backbone curve of pinching hysteresis model.[10]

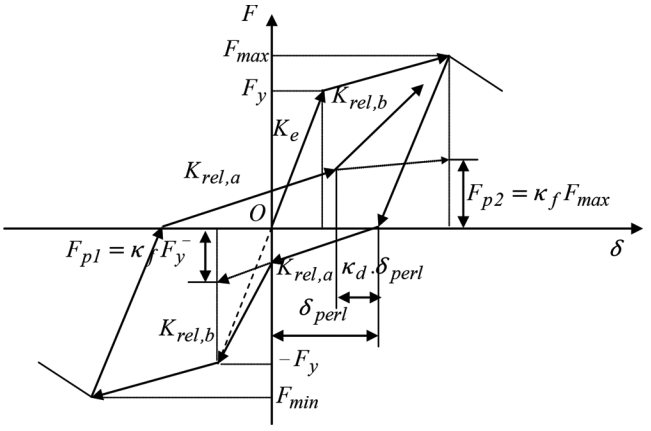

Fig. 13—Load-deflection diagram of pinching hysteresis model in absence of deterioration.[10]

The normalized dissipated energy $\bar{E}_{h,n}$ at the equivalent n-th cycle number is

$$\bar{E}_{h,n} = \alpha + (1-\alpha)e^{\beta(1-n)} \quad (17)$$

Here, $(1 - \alpha)$ is the loss of energy dissipation capacity for larger values of n, and β is the rate of loss of dissipated energy.

The backbone curve of pinching hysteresis model by Ibarra et al.[10] has three control points at yield strength F_y, peak strength F_c, residual strength F_r ($F_r = \lambda F_y$), and the respective displacements δ_y, δ_c, and δ_r, as shown in Fig. 12. K_e, K_s, and K_c are elastic stiffness, post-yielding stiffness ($K_s = \alpha_s K_e$) and post-capping (negative) stiffness ($K_c = \alpha_c K_e$), respectively, and α_s, α_c, and λ are constants. The primary curve of the pinching hysteresis model in the absence of deterioration is shown in Fig. 13. Cyclic deterioration β_i in excursion i is defined as follows in terms of dissipated hysteretic energy E_i in excursion i.

$$\beta_i = \left\langle E_i \middle/ \left(E_t - \sum_{j=1}^{i} E_j \right) \right\rangle^c \quad (18)$$

where $\sum E_j$ is hysteretic energy dissipated in all previous excursions; E_t is hysteretic energy dissipation capacity

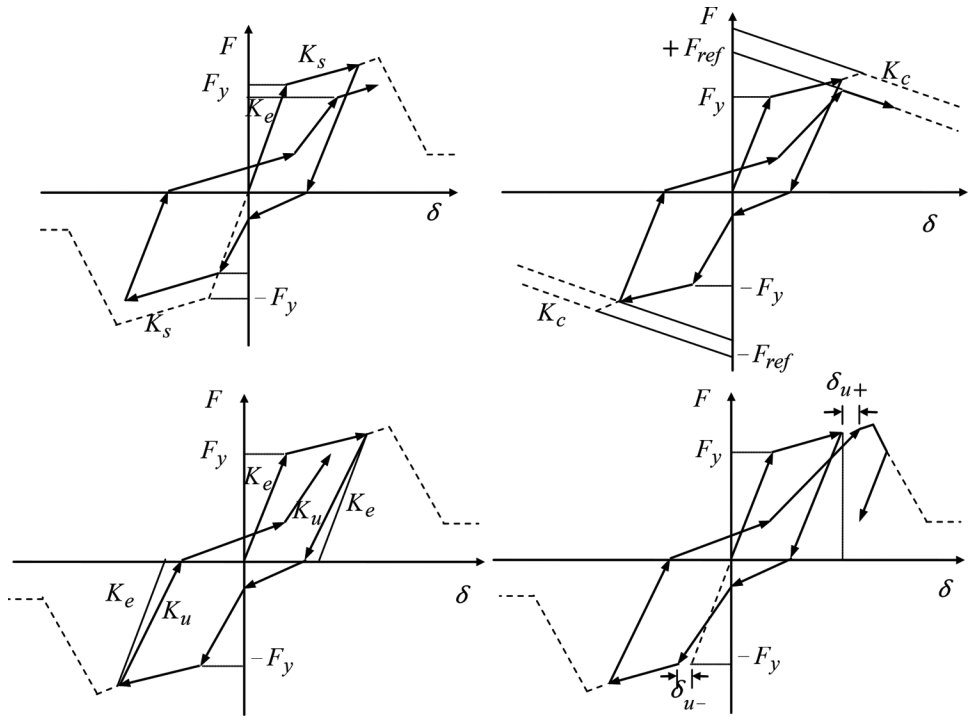

Fig. 14—Four deterioration modes of pinching hysteresis model[10]: (a) basic strength deterioration; (b) post-capping strength deterioration; (c) unloading stiffness deterioration; and (d) accelerated reloading stiffness deterioration.

($E_t = F_y\delta_y$); and c is rate of deterioration rate, ranging between 1 and 2. The expressions of the basic strength, post-capping strength, unloading stiffness, and accelerated reloading stiffness degradations (shown in Fig. 14) are mentioned as follows.

$$F_{y,i} = (1 - \beta_{s,i})F_{y,i-1} \tag{19}$$

$$K_{s,i} = (1 - \beta_{s,i})K_{s,i-1} \tag{20}$$

$$F_{ref,i} = (1 - \beta_{c,i})F_{ref,i-1} \tag{21}$$

$$K_{u,i} = (1 - \beta_{k,i})K_{u,i-1} \tag{22}$$

$$\delta_{t,i} = (1 + \beta_{a,i})\delta_{t,i-1} \tag{23}$$

where $F_{ref,i}$ is intersection of vertical axis and projected post-capping branch for excursion i; $\beta_{s,i}$, $\beta_{c,i}$, $\beta_{k,i}$, and $\beta_{a,i}$ are deterioration rates of basic strength, post-capping strength, unloading stiffness, and accelerated reloading stiffness, respectively, in excursion i; and $\delta_{t,i}$ is incremented maximum displacement after excursion i.

Smooth hysteresis models

Bouc[11] suggested a smoothly varying hysteresis model for a single-degree-of-freedom (SDOF) system under forced vibration. Then, Baber and Wen[12] and Baber and Noori[13] extended the model with the inclusion of stiffness and strength degradation, and pinching effects, respectively. The equation of motion for a SDOF system, as shown in Fig. 15, is presented as follows

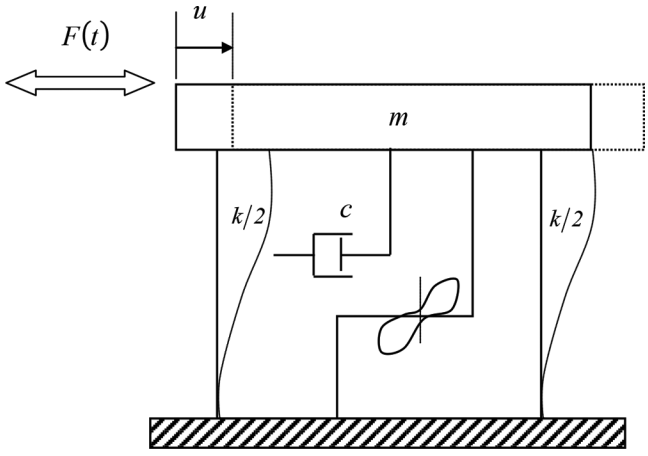

Fig. 15—Schematic model of single-degree-of-freedom hysteretic system.

$$m\ddot{u} + c\dot{u} + F_T\left[u(t), z(t), t\right] = F(t) \tag{24}$$

where u is relative displacement of mass m with respect to ground motion; c is linear viscous damping coefficient; $F_T[u(t),z(t),t]$ is non-damping restoring force consisting of linear restoring force αku and hysteretic restoring force $(1 - \alpha)kz$; α is ratio of final asymptote tangent stiffness k_f to initial stiffness k_i with magnitudes 1 for a linear system and 0 for a nonlinear system; and $F(t)$ is time-dependent forcing function. Dividing both sides of Eq. (24) by m

$$\ddot{u} + 2\xi_0\omega_0\dot{u} + \alpha\omega_0^2 u + (1-\alpha)\omega_0^2 z = f(t) \tag{25}$$

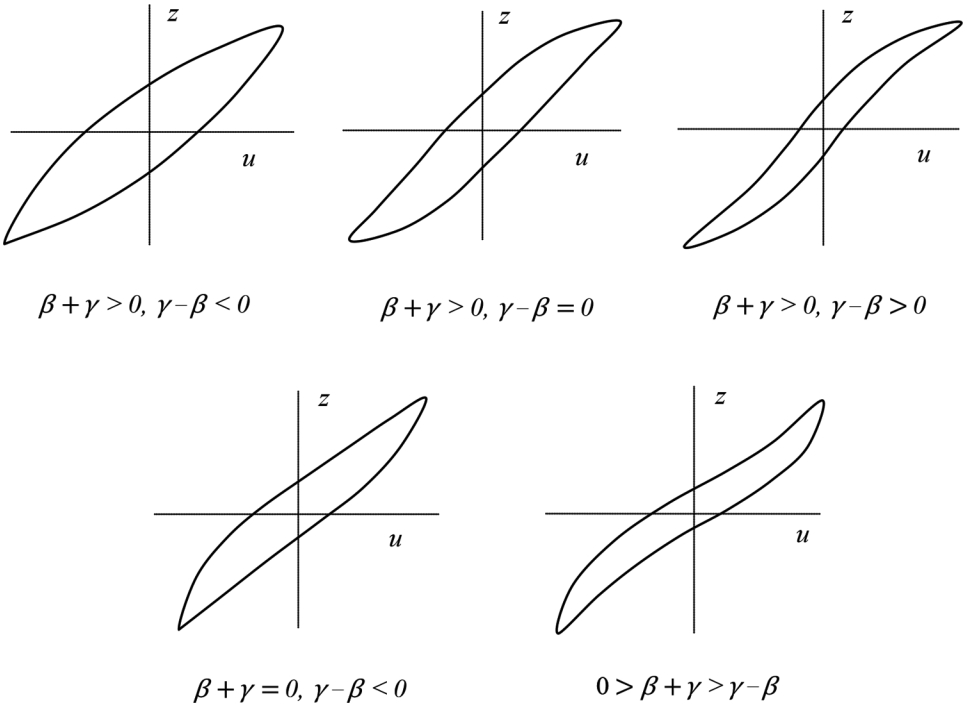

Fig. 16—Possible shapes of hysteresis loops under different combinations of β and γ for n *= 1.*[12]

where ξ_0 is the linear damping ratio, $c/2\sqrt{k_i m}$; ω_0 is the pre-yield system natural frequency $\sqrt{k_i/m}$; and $f(t)$ is the mass-normalized forcing function. Hysteretic restoring force is a function of hysteretic displacement z and, thus, the relationship between z and u is

$$\dot{z} = h(z)\frac{A\dot{u} - \nu\left(\beta|\dot{u}||z|^{n-1}z + \gamma\dot{u}|z|^{n}\right)}{\eta} \tag{26}$$

where A is tangent stiffness; β, γ, and n are hysteretic shape parameters; ν and η are strength and stiffness degradation parameters, respectively; and $h(z)$ is pinching function. For a non-pinching and non-degrading system, hysteresis stiffness is zero at local maximum or minimum—that is, the point on the load-deflection curve where velocity changes its sign. So, at an infinitesimal distance dz away from z_{max}, where velocity is close to but not equal to zero and $\dot{z}_{max} \approx \dot{z}$

$$\dot{z}_{max} \approx 0 = A\dot{u} - \nu\left(\beta|\dot{u}||z|^{n-1}z + \gamma\dot{u}|z|^{n}\right)$$

$$z_{max} = \pm\{A/\nu(\beta+\gamma)\}^{1/n} \tag{27}$$

Inclusion of variation of A can contribute to the versatility of the model. However, A is redundant as both hysteretic stiffness and force can be varied by stiffness ratio and hysteresis shape parameters. Thus, for simplicity, the magnitude of A is set to unity.

Hysteresis shape parameters β, γ, and n determine basic hysteresis shape. β and γ individually influence hysteretic strength and stiffness inversely while they jointly influence softening or hardening of hysteresis loops. n controls sharpness of transition from initial to asymptotic slope. For n = 1, effects of combined β and γ on hysteresis loops shown in Fig. 16 are as follows.

i) $\left.\begin{matrix}\beta+\gamma>0\\ \gamma-\beta<0\end{matrix}\right\rangle$ weak softening

ii) $\left.\begin{matrix}\beta+\gamma>0\\ \gamma-\beta=0\end{matrix}\right\rangle$ weak softening on loading, mostly linear unloading

iii) $\left.\begin{matrix}\beta+\gamma>\gamma-\beta\\ \gamma-\beta>0\end{matrix}\right\rangle$ strong softening on loading and unloading, narrow loop

iv) $\left.\begin{matrix}\beta+\gamma=0\\ \gamma-\beta<0\end{matrix}\right\rangle$ weak hardening

v) $\left.\begin{matrix}0>\beta+\gamma\\ \beta+\gamma>\gamma-\beta\end{matrix}\right\rangle$ strong hardening

Hysteretic energy ε, defined as irrecoverable strain energy absorbed by hysteretic element, is used to approximate structural degradation and pinching. Although the total strain energy consists of irrecoverable hysteretic energy and recoverable strain energy, the latter is quite small compared to the former. Thus, hysteretic energy is considered approximately equal to total energy and expressed as continuous integral of hysteretic force $f(t)$ over total displacement u.

$$\begin{aligned}\varepsilon(t) &= \int_{u(0)}^{u(t)} f\cdot du = (1-\alpha)\omega_0^{\,2}\int_{u(0)}^{u(t)} z(u,t)\cdot du\cdot\frac{du}{dt}\\ &= (1-\alpha)\omega_0^{\,2}\int_0^t z(u,t)\cdot\dot{u}(t)\cdot dt\end{aligned} \tag{28}$$

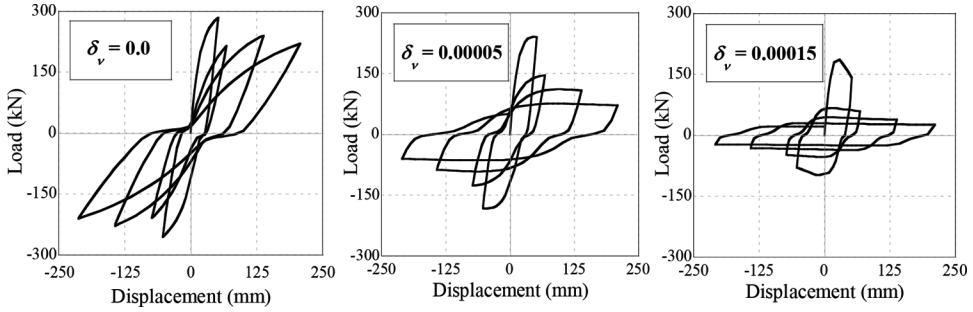

Fig. 17—Effect of varying strength degradation rate δ_v on hysteresis loops when all other parameters and input functions are the same. (Note: 1 kN = 0.225 kip; 1 mm = 0.0394 in.)

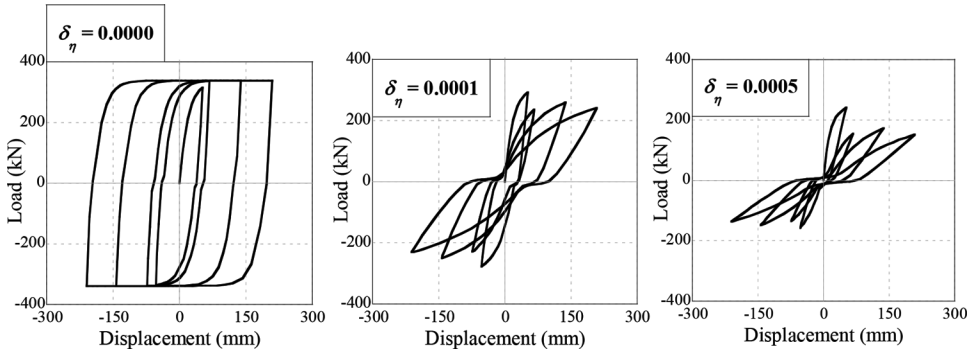

Fig. 18—Effect of varying stiffness degradation rate δ_η on hysteresis loops when all other parameters and input functions are the same. (Note: 1 kN = 0.225 kip; 1 mm = 0.0394 in.)

A gradual decrease in structural strength at the same displacement level is termed "strength degradation". Progressive loss of structural stiffness in each loading cycle is defined as stiffness degradation. Strength and stiffness degradation parameters ν and η, respectively, are functions of hysteretic energy ε, strength degradation rate δ_ν, and stiffness degradation rate δ_η, as follows

$$\nu(\varepsilon) = 1 + \delta_\nu \varepsilon \tag{29}$$

$$\eta(\varepsilon) = 1 + \delta_\eta \varepsilon \tag{30}$$

Effects of change in magnitudes of δ_ν and δ_η on hysteresis loops are shown in Fig. 17 and 18, respectively, when the input function and remaining model parameters are same. For zero magnitudes of δ_ν and δ_η, structure does not degrade. With an increase in δ_η, both hysteretic force and stiffness degrade while increase in δ_ν reduces the hysteretic force only.

The expression for pinching function $h(z)$ is as follows

$$h(z) = 1 - \zeta_1 e^{-(z\,\mathrm{sgn}(\dot{u}) - q z_{max})^2 / \zeta_2^2} \tag{31}$$

where ζ_1 and ζ_2 are pinching severity and pinching spread parameters, respectively; and q is pinching level as a fraction of z_{max}. Both ζ_1 and ζ_2 vary with hysteretic energy ε as follows

$$\zeta_1(\varepsilon) = \zeta_s \left\langle 1 - e^{(-p\varepsilon)} \right\rangle \tag{32}$$

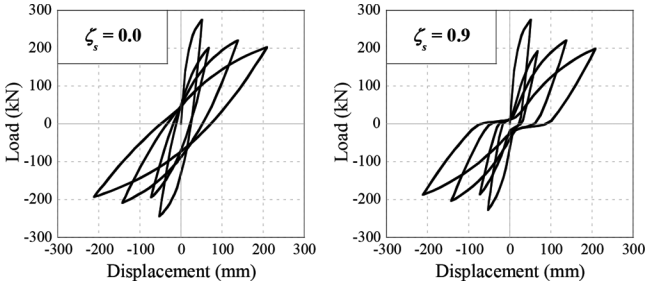

Fig. 19—Effect of pinching on hysteresis loops. (Note: 1 kN = 0.225 kip; 1 mm = 0.0394 in.)

$$\zeta_2(\varepsilon) = (\psi + \delta_\psi)(\lambda + \zeta_1) \tag{33}$$

where p is rate of initial drop in slope; ζ_s is total slip; ψ is total pinching; δ_ψ is pinching spread rate; and λ is rate of change of ζ_2 with change of ζ_1. Effect of pinching on hysteresis behavior with changing ζ_s is shown in Fig. 19.

Based on experimental results of RC structures under repeated cyclic loading, Sengupta et al.[14-17] modified original Bouc-Wen-Baber-Noori (BWBN) model by incorporating displacement-based stiffness ratio α in terms of initial stiffness ratio α_0 and absolute maximum displacement D_{max}.

$$\alpha = \alpha_0 e^{(-0.1 Dmax))} \tag{34}$$

The stiff set of ordinary differential equations involved in the mathematical expressions of the BWBN model requires a suitable solver. Because the hysteretic response is not only dependent on individual parameter magnitude, but also on

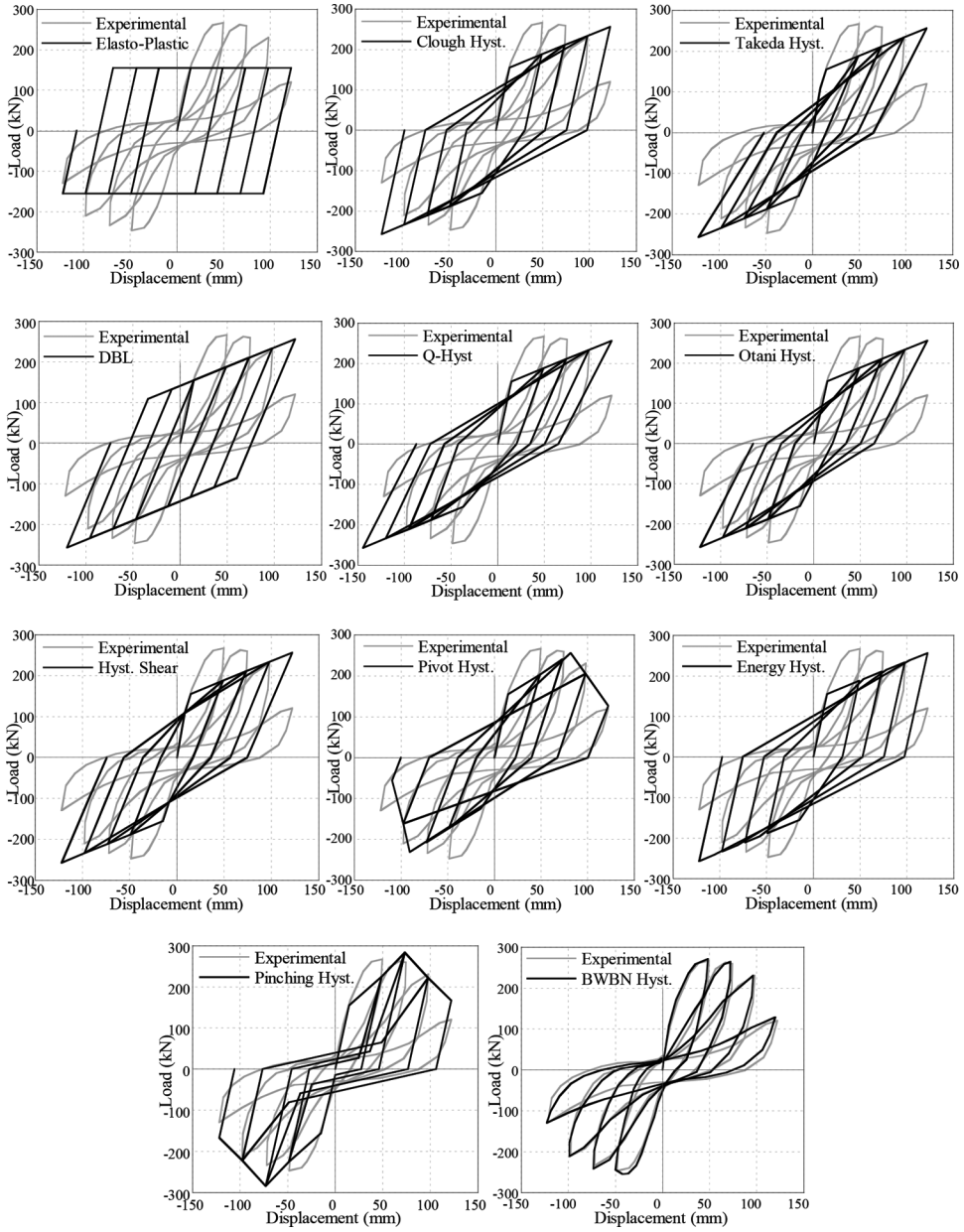

Fig. 20—Experimental and hysteresis load-deformation plots of RC interior beam-column joint specimen PEER14. (Note: 1 kN = 0.225 kip; 1 mm = 0.0394 in.)

their interaction, a genetic algorithm is used in this study for systematic parameter estimation of the BWBN model.[14-17]

COMPARISON OF HYSTERESIS MODELS WITH EXPERIMENTAL RESULTS

Based on the literature review on hysteresis models, it is observed that elasto-plastic[1] and degrading bilinear models[4] are unable to represent realistic structural hysteresis response. The Clough model[2] does not incorporate pinching effect. Q-hysteresis[5] and Otani models[6] impractically consider concrete section elastic until yielding while nonlinearity initiates after appearance of cracks. Performances of Takeda model,[3] pivot hysteresis,[7] and hysteresis shear[8] models are poor compared to the number of rules. Energy-based hysteresis model[9] cannot perform satisfactorily at larger cycle numbers, as pinching effect is not included in the model. The contribution of four deterioration modes of the pinching hysteresis model[10] on structural response is not defined adequately.

Thus, to assess performance of the hysteresis models with respect to the experimental load-deformation plots, a series of RC beam-column joint and wall specimens are accumulated from the literature[18-34] for construction of hysteresis load-deformation plots using the existing hysteresis models. The test specimens (34 beam-column joints and 56 shear walls) are selected from the literature such that wide variations in terms of structural features, material properties, and loading characteristics are covered to enhance the effectiveness of the hysteresis model performance assessment. The experimental and hysteresis load-deformation responses of RC interior beam-column joint specimen PEER14, exterior beam-column joint specimen EJ4, wall specimen C1.5K

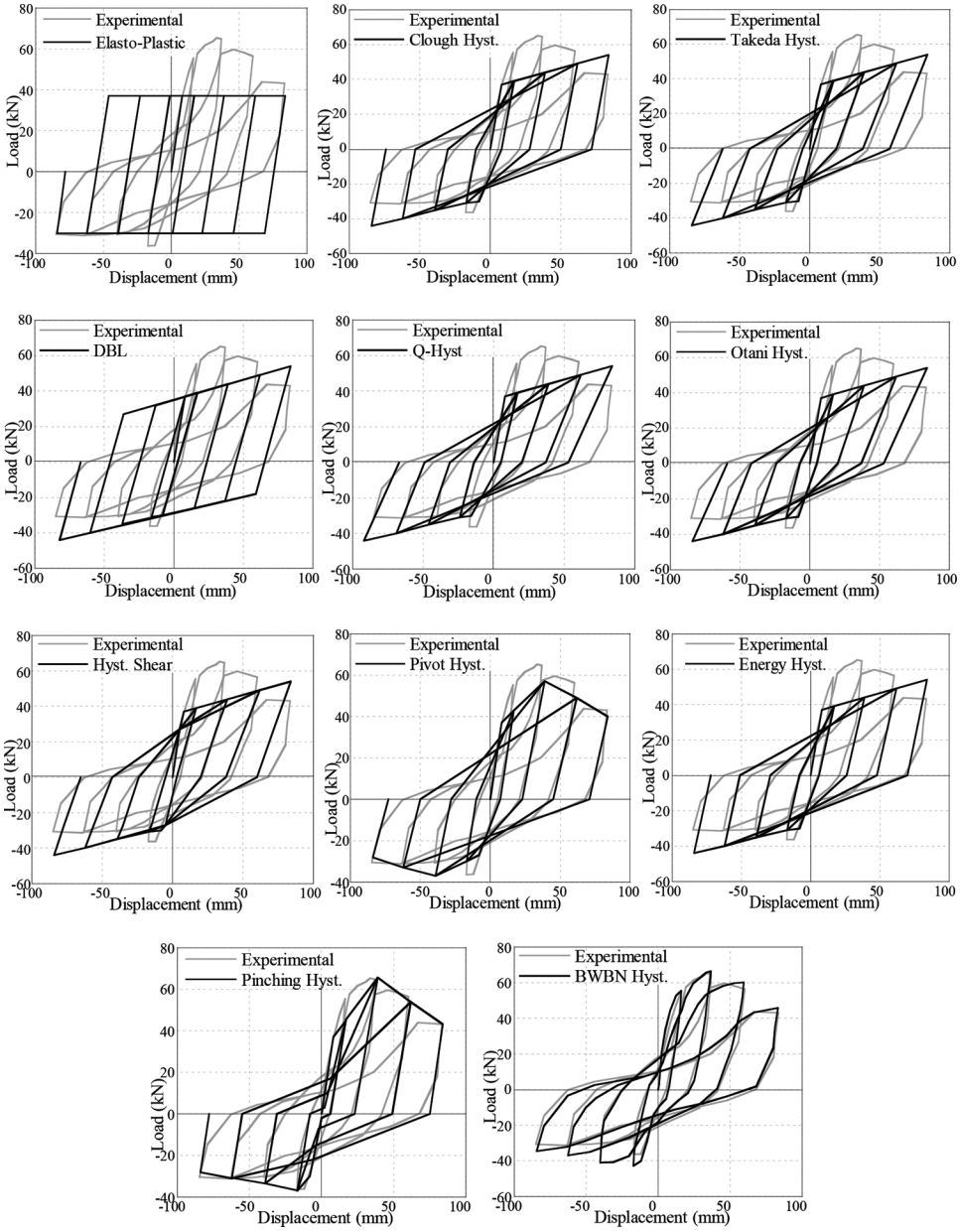

Fig. 21—Experimental and hysteresis load-deformation plots of reinforced concrete exterior beam-column joint Specimen EJ4. (Note: 1 kN = 0.225 kip; 1 mm = 0.0394 in.)

with rectangular cross section, and wall specimen MW3 with flanged cross section are presented in Fig. 20, 21, 22, and 23, respectively. Reinforced concrete interior beam-column joint specimen PEER14 and wall specimen MW3 exhibit pinched and thinner hysteresis loops, while exterior beam-column joint specimen EJ4 and wall specimen C1.5K exhibit non-pinched and fatter hysteresis loops. From the comparison plots, it can be observed that the BWBN hysteresis model[11-17] performs reasonably well to capture both pinched and non-pinched hysteresis response. Among the polygonal hysteresis models, the pinching hysteresis model[10] performs well with respect to the experimental load-deformation plots for both pinched and non-pinched hysteresis response. The pinching hysteresis model[10] can capture pinched hysteresis response much better than non-pinched hysteresis response. Elasto-plastic[1] and degrading bilinear models[4] cannot capture pinched or non-pinched hysteresis response with requisite accuracy. The remaining models—Clough model,[2] Takeda model,[3] Q-hysteresis model,[5] Otani model,[6] pivot hysteresis model,[7] hysteresis shear model,[8] and energy-based hysteresis model[9]—cannot capture pinched hysteresis response well. However, all these models can capture non-pinched hysteresis response adequately. Additionally, the Takeda model,[3] Q-hysteresis model,[5] Otani model,[6] pivot hysteresis model[7] and hysteresis shear model[8] can also capture structural hysteresis response with mild pinching behavior.

Because hysteretic energy is a measure to quantify the performance of the hysteresis models, experimental and model hysteretic energy are computed from experimental and hysteresis load-deformation plots of beam-column joint and wall specimens. The correlation and average deviation (in %) between the experimental and model hyster-

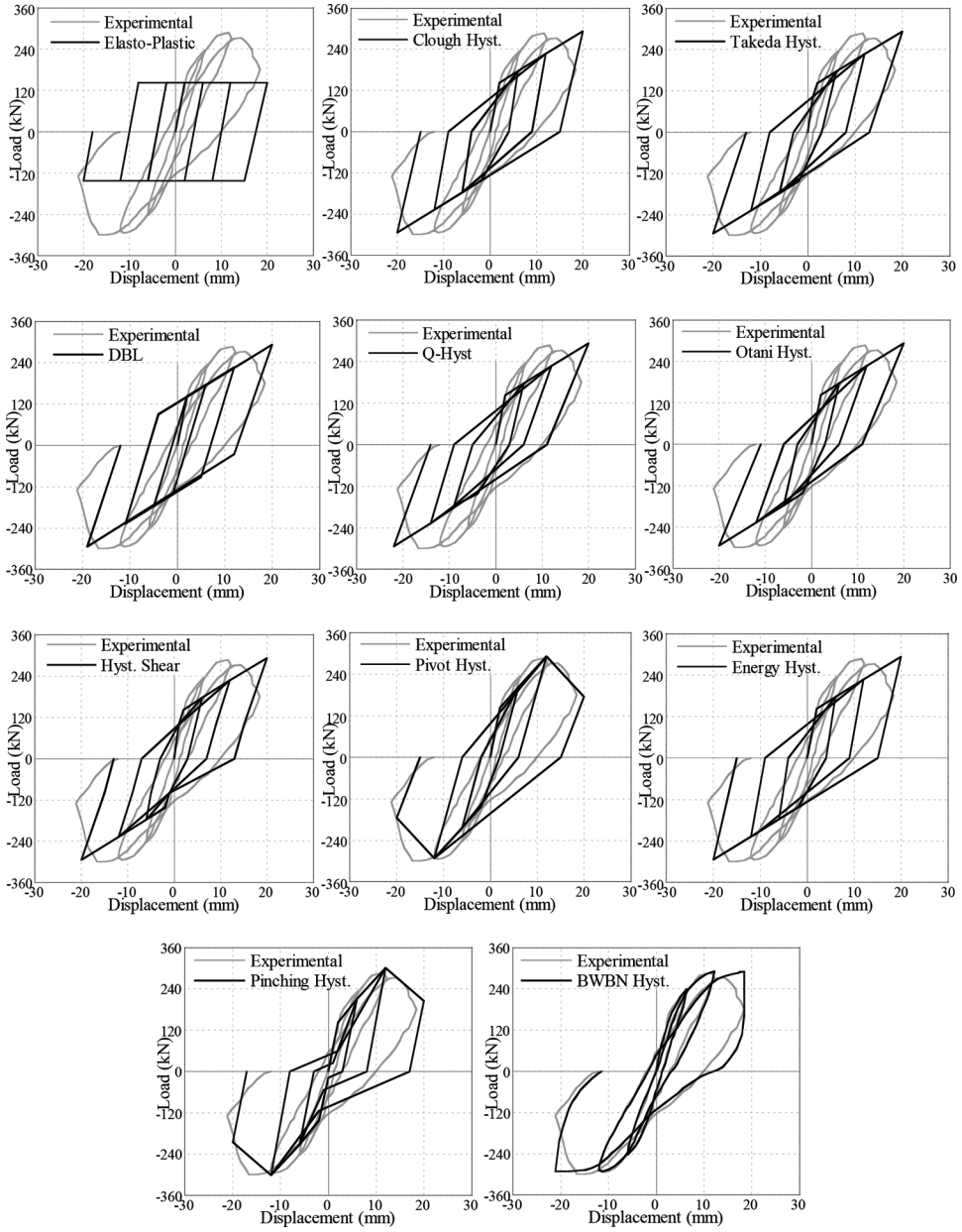

Fig. 22—Experimental and hysteresis load-deformation plots of reinforced concrete wall Specimen C1.5K with rectangular cross section. (Note: 1 kN = 0.225 kip; 1 mm = 0.0394 in.)

etic energy of beam-column joint and wall specimens are presented in Fig. 24 and 25, respectively. Figure 24 shows that the correlation between the experimental and model hysteretic energy is maximum for the BWBN model[11-17] with minimum scatter, while Fig. 25 shows that average deviation in hysteretic energy obtained from the BWBN model[11-17] is only 3% from experimental hysteretic energy. Average deviations in hysteretic energy obtained from pinching hysteresis model,[10] Otani model,[6] Takeda model,[3] hysteresis shear model[8] and Q-hysteresis model[5] are 23.55%, 29.61%, 32.87%, 35.24%, and 41.90%, respectively, from experimental hysteretic energy. Similarly, average deviations in hysteretic energy obtained from degrading bilinear model,[4] pivot hysteresis model,[7] energy-based hysteresis model,[9] Clough model,[2] and elasto-plastic model[1] are 46.28%, 76.5%, 80.52%, 81.09%, and 130.17%, respectively, from experimental hysteretic energy.

CONCLUSIONS

Based on the literature review conducted on hysteresis modeling of RC structural components in the present paper, the following conclusions are drawn:

1. Elasto-plastic[1] and degrading bilinear models[4] are unable to represent realistic structural hysteresis response. The Clough model[2] does not incorporate pinching effect. Q-hysteresis[5] and Otani models[6] impractically consider concrete section elastic until yielding with nonlinearity initiating after the appearance of cracks. The performances of the Takeda model,[3] pivot hysteresis model,[7] and hysteresis shear model[8] are poor compared to number of rules involved. The performance of the energy-based hysteresis model[9] is not

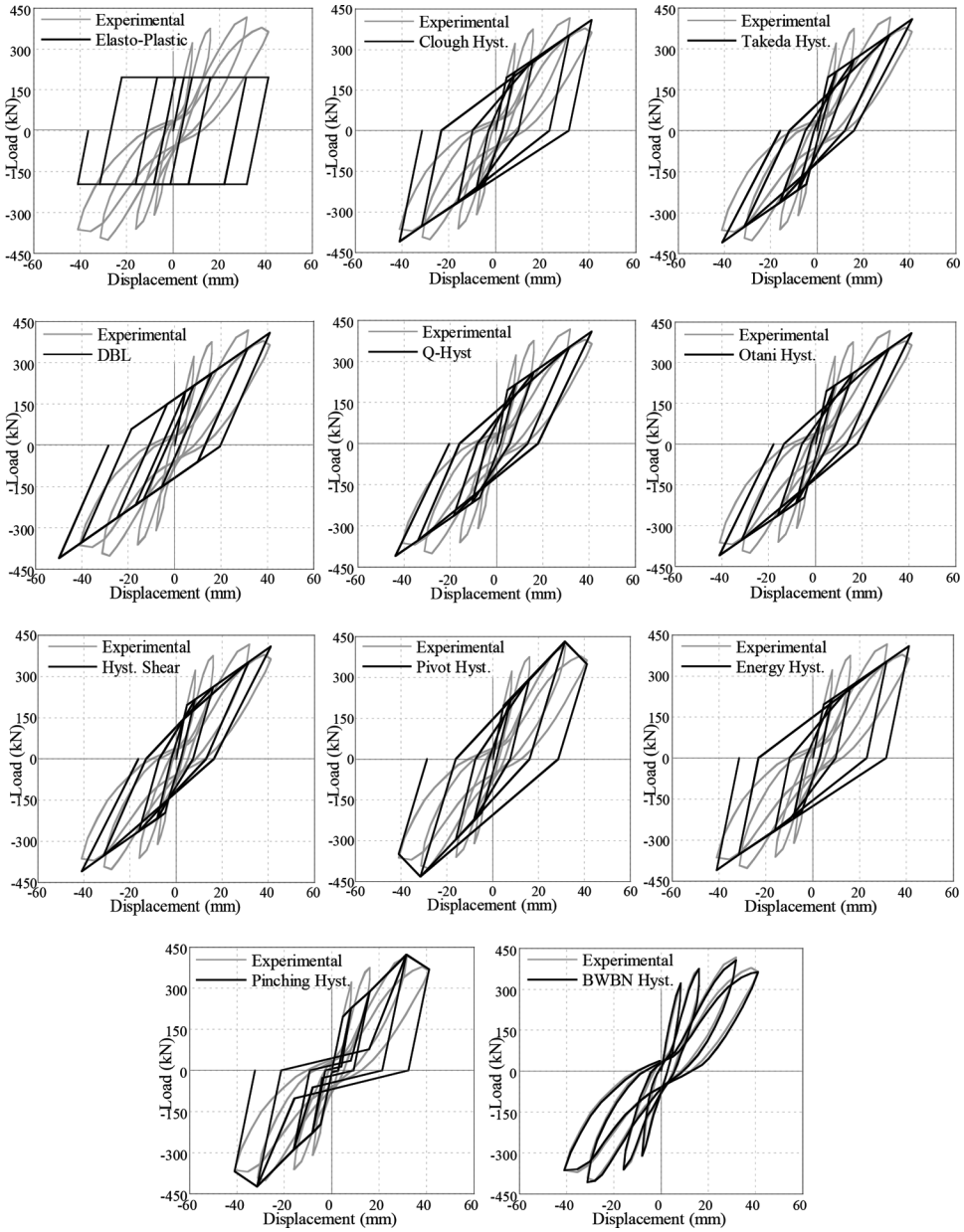

Fig. 23—Experimental and hysteresis load-deformation plots of reinforced concrete wall Specimen MW3 with flanged cross section. (Note: 1 kN = 0.225 kip; 1 mm = 0.0394 in.)

quite satisfactory at larger cycle numbers, as the pinching effect is not included in the model. Contribution of four deterioration modes of pinching hysteresis model[10] on the structural behavior is not defined adequately.

2. Bouc-Wen-Baber-Noori (BWBN) hysteresis model[11-17] uses several parameters to capture various aspects of RC structures under repeated cyclic loading, such as structural degradation, pinching, softening and hardening. However, the stiff set of ordinary differential equations involved in the mathematical expressions of the model requires a suitable solver. Because structural hysteresis response is dependent on individual and combined magnitudes of parameters, a system identification tool is also necessary for parameter estimation. A genetic algorithm is used in this study for systematic parameter estimation of the BWBN model.[14-17]

3. From the comparison study between the hysteresis models and experimental results of RC beam-column joint and wall specimens, it is quite evident that the BWBN model[11-17] performs better than other hysteresis models for both pinched and non-pinched hysteresis response. The hysteresis loops obtained from BWBN Model[11-17] closely match the experimental load-deformation plots, and the average difference between the experimental and model hysteretic energy is only 3%. After the BWBN model,[11-17] the pinching hysteresis model[10] performs well for both pinched and non-pinched hysteresis response. The pinching hysteresis model[10] can capture pinched hysteresis response much better than non-pinched hysteresis response. Elas-to-plastic[1] and degrading bilinear models[4] cannot capture pinched or non-pinched hysteresis response with requisite accuracy. The remaining models—Clough model,[2] Takeda

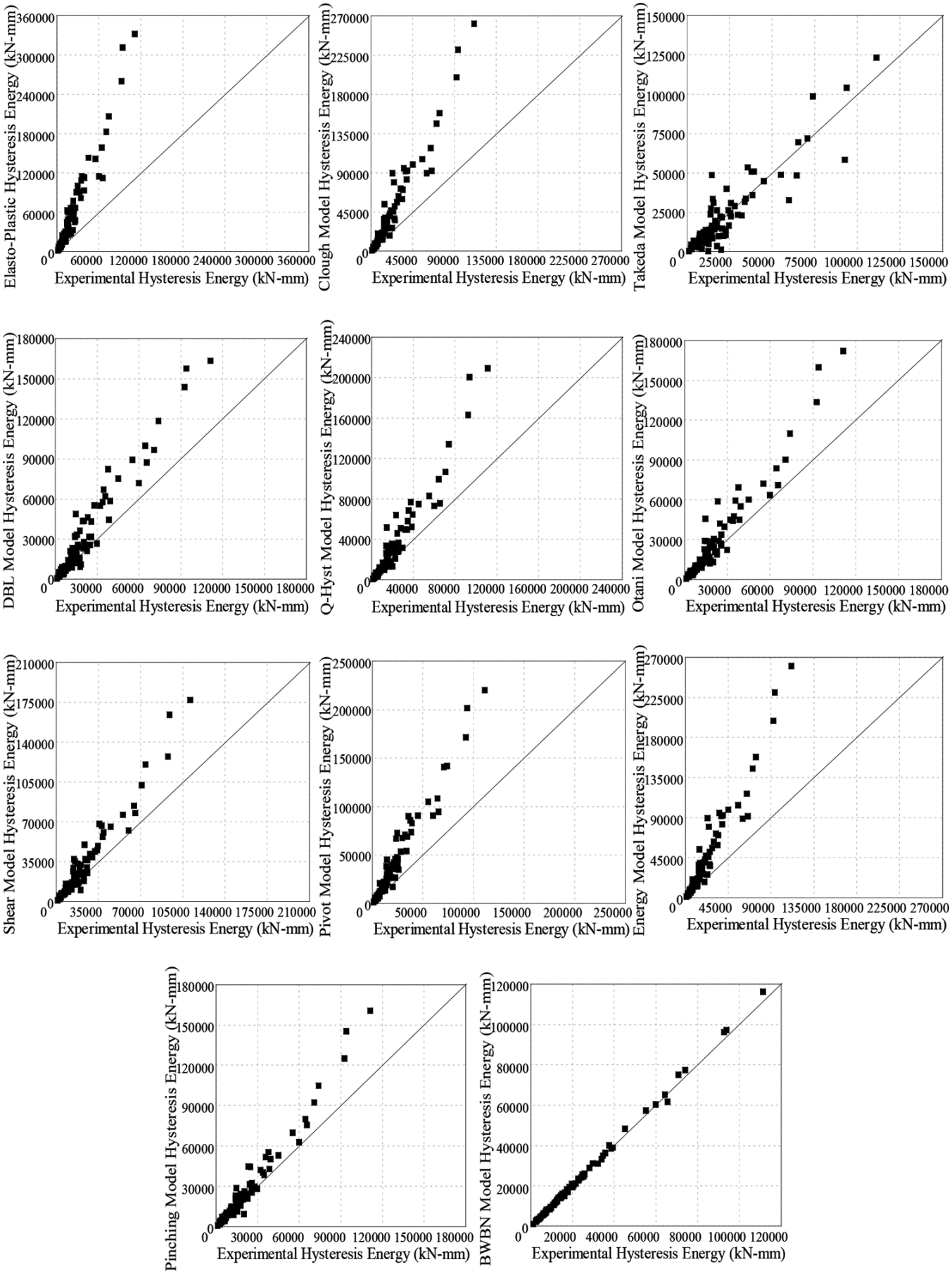

Fig. 24—Correlation study between hysteretic energy obtained from hysteresis models and experimental results. (Note: 1 kN = 0.225 kip; 1 mm = 0.0394 in.)

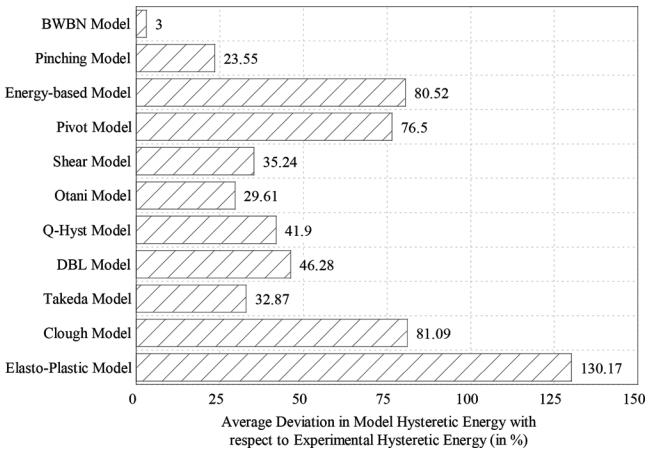

Fig. 25—Average deviations in hysteretic energy (in percent) obtained from hysteresis models with respect to experimental results.

model,[3] Q-hysteresis model,[5] Otani model,[6] pivot hysteresis Model,[7] hysteresis shear model[8] and energy-based hysteresis model[9]—cannot capture pinched hysteresis response well. However, all these models can capture represent non-pinched hysteresis response adequately. Additionally, the Takeda model,[3] Q-hysteresis model,[5] Otani model,[6] pivot hysteresis model[7] and hysteresis shear model[8] can also capture structural hysteresis response with mild pinching behavior.

4. Future research can be conducted on the simplification of the BWBN model[11-17] by reducing the number of analytical parameters for predicting hysteresis behavior of RC structures. An optimum hysteresis model must be deduced such that the overall performance of the model remains satisfactory with minimum computational complicacy involved in the methodology.

AUTHOR BIOS

Piyali Sengupta *is a Research Fellow in School of Civil and Environmental Engineering at National University of Singapore, Singapore. She received her PhD from Nanyang Technological University, Singapore. Her research interests include hysteresis modeling and performance assessment of reinforced concrete structures under dynamic loading.*

ACI member **Bing Li** *is an Associate Professor in the School of Civil and Environmental Engineering at Nanyang Technological University, Singapore. He received his PhD from the University of Canterbury, Christchurch, New Zealand. He is a member of ACI Committee 377, Performance-Based Structural Integrity & Resilience of Concrete Structures; and Joint ACI-ASCE Committees 352, Joints and Connections in Monolithic Concrete Structures; and 441, Reinforced Concrete Columns.*

REFERENCES

1. Veletsos, A. S.; Newmark, N. M.; and Chelapati, C. V., "Deformation Spectra for Elastic and Elastoplastic Systems subjected to Ground Shock and Earthquake Motions," *Proceedings of 3rd World Conference on Earthquake Engineering*, V. II, 1965, pp. 663-682.

2. Clough, R. W., and Johnston, S. B., "Effect of Stiffness Degradation on Earthquake Ductility Requirements," *Proceedings of 2nd Japan National Conference on Earthquake Engineering*, 1966, pp. 227-232.

3. Takeda, T.; Sozen, M. A.; and Nielson, N. N., "Reinforced Concrete Response to Simulated Earthquakes," *Journal of the Structural Division*, ASCE, V. 96, 1970, pp. 2557-2573.

4. Imbeault, F. A., and Nielsen, N. N., "Effect of Degrading Stiffness on the Response of Multistory Frames Subjected to Earthquakes," *Proceedings of 5th World Conference on Earthquake Engineering*, 1973, pp. 1756-1765.

5. Saidi, M., and Sozen, M. A., "Simple and Complex Models for Nonlinear Seismic Response of Reinforced Concrete Structures," *A Report to the National Science Foundation*, University of Illinois at Urbana-Champaign, Champaign, IL, Aug. 1979, 204 pp.

6. Otani, S., "Nonlinear Dynamic Analysis of Reinforced Concrete Building Structures," *Canadian Journal of Civil Engineering*, V. 7, No. 2, 1980, pp. 333-344. doi: 10.1139/l80-041

7. Ozcebe, G., and Saatcioglu, M., "Hysteresis Shear Models for Reinforced Concrete Members," *Journal of Engineering Mechanics*, V. 115, No. 1, 1989, pp. 132-148.

8. Dowell, R. K.; Seible, F.; and Wilson, E. L., "Pivot Hysteresis Model for Reinforced Concrete Members," *ACI Structural Journal*, ASCE, V. 95, No. 5, Sept.-Oct. 1998, pp. 607-617.

9. Sucuoglu, H., and Erberik, A., "Energy-Based Hysteresis and Damage Models for Deteriorating Systems," *Earthquake Engineering & Structural Dynamics*, V. 33, No. 1, 2004, pp. 69-88. doi: 10.1002/eqe.338

10. Ibarra, L. F.; Medina, R. A.; and Krawinkler, H., "Hysteretic Models that incorporate Strength and Stiffness Deterioration," *Earthquake Engineering & Structural Dynamics*, V. 34, No. 12, 2005, pp. 1489-1511. doi: 10.1002/eqe.495

11. Bouc, R., "Forced Vibration of Mechanical Systems with Hysteresis," *Proceedings of the 4th Conference on Nonlinear Oscillation*, Prague, Czechoslovakia, 1967, pp. 315.

12. Baber, T. T., and Wen, Y. K., "Random Vibrations of Hysteretic Degrading Systems," *Journal of Engineering Mechanics*, ASCE, V. 107, No. 6, 1981, pp. 1069-1087.

13. Baber, T. T., and Noori, M. N., "Random Vibration of Degrading Pinching Systems," *Journal of Engineering Mechanics*, ASCE, V. 111, No. 8, 1985, pp. 1010-1026. doi: 10.1061/(ASCE)0733-9399(1985)111:8(1010)

14. Sengupta, P., and Li, B., "Modified Bouc-Wen Model for Hysteresis Behavior of RC Beam-Column Joints with Limited Transverse Reinforcement," *Engineering Structures*, V. 46, 2013, pp. 392-406. doi: 10.1016/j.engstruct.2012.08.003

15. Sengupta, P., and Li, B., "Hysteresis Behavior of Reinforced Concrete Walls," *Journal of Structural Engineering*, ASCE, V. 140, No. 7, 2014, pp. 1-18. doi: 10.1061/(ASCE)ST.1943-541X.0000927

16. Sengupta, P., and Li, B., "Seismic Fragility Evaluation of Lightly Reinforced Concrete Beam-Column Joints," *Journal of Earthquake Engineering*, V. 18, No. 7, 2014, pp. 1102-1128. doi: 10.1080/13632469.2014.919890

17. Sengupta, P., and Li, B., "Seismic Fragility Evaluation of Reinforced Concrete Structural Walls," *Journal of Earthquake Engineering*, ASCE, doi: 10.1080/13632469.2015.1104755

18. Hakuto, S.; Park, R.; and Tanaka, H., "Seismic Load Tests on Interior and Exterior Beam-Column Joints with Substandard Reinforcing Details," *ACI Structural Journal*, V. 97, No. 1, Jan.-Feb. 2000, pp. 11-25.

19. Liu, A., "Seismic Assessment and Retrofit of Pre-1970s Reinforced Concrete Frame Structures," PhD dissertation, University of Canterbury, Christchurch, New Zealand, 2001, 420 pp.

20. Walker, S. G., "Seismic Performance of Existing Reinforced Concrete Beam-Column Joints," MSCE thesis, Department of Civil Engineering, University of Washington, Seattle, WA, 2001, 308 pp.

21. Alire, D. A., "Seismic Evaluation of Existing Unconfined Reinforced Concrete Beam-Column Joints," MSCE thesis, Department of Civil Engineering, University of Washington, Seattle, WA, 2002, 291 pp.

22. Pessiki, S. P.; Conley, C. H.; Gergely, P.; and White, R. N., "Seismic Behavior of Lightly-RC Column and Beam-Column Joint Details," *Technical Report NCEER-90-0014*, 1990, pp. 231.

23. Joh, O.; Goto, Y.; and Shibata, T., "Influence of Transverse Joint and Beam Reinforcement and Relocation of Plastic Hinge Region on Beam-Column Joint Stiffness Deterioration," *Design of Beam-Column Joints for Seismic Resistance*, SP-123, J. O. Jirsa, ed., American Concrete Institute, Farmington Hills, MI, 1991, pp. 187-223.

24. Joh, O.; Goto, Y.; and Shibata, T., "Behavior of Reinforced Concrete Beam-Column Joints with Eccentricity," *Design of Beam-Column Joints for Seismic Resistance*, SP-123, J. O. Jirsa, ed., American Concrete Institute, Farmington Hills, MI, 1991, pp. 317-357.

25. Pantelides, C. P.; Hansen, J.; Nadauld, J. D.; and Reaveley, L. D., "Assessment of Reinforced Concrete Building Exterior Joints with Substandard Details," *PEER Report 2002/18*, University of California, Berkeley, Berkeley, CA, May 2002, 103 pp.

26. Pantelides, C. P.; Clyde, C.; and Reaveley, L. D., "Performance-Based Evaluation of Reinforced Concrete Building Exterior Joints for Seismic Excitation," *Earthquake Spectra*, V. 18, No. 3, 2002, pp. 449-480. doi: 10.1193/1.1510447

27. Hirosawa, M., "Past Experimental Results on Reinforced Concrete Shear Walls and Analysis on Them," Kenchiku Kenkyu Shiryo, No. 6, Building Research Institute, Ministry of Construction, Tokyo, Japan, 1975, 277 pp.

28. Greifenhagen, C., "Seismic Behavior of Lightly Reinforced Concrete Squat Shear Walls," PhD thesis, École Polytechnique Fédérale de Lausanne (EPFL), Switzerland, 2006, 164 pp.

29. Hidalgo, P. A.; Ledezma, C. A.; and Jordan, R. M., "Seismic Behavior of Squat Reinforced Concrete Shear Walls," *Earthquake Spectra*, V. 18, No. 2, 2002, pp. 287-308. doi: 10.1193/1.1490353

30. Massone, L. M., "RC Wall Shear-Flexure Interaction: Analytical and Experimental Responses," PhD dissertation, Department of Civil and Environmental Engineering, University of California, Los Angeles, Los Angeles, CA, 2006, 398 pp.

31. Kuang, J. S., and Ho, Y. B., "Seismic Behavior and Ductility of Squat Reinforced Concrete Shear Walls with Nonseismic Detailing," *ACI Structural Journal*, V. 105, No. 2, Mar.-Apr. 2008, pp. 225-231.

32. Maier, J., and Thürlimann, B., "Bruchversuche an Stahlbetonscheiben," Institut für Baustatik und Konstruktion, ETH Zürich, Zürich, Switzerland, 1985, 130 pp.

33. Sato, S.; Ogata, Y.; Yoshizaki, S.; Kanata, K.; Yamaguchi, T.; Nakayama, T.; Inada, Y.; and Kadoriku, J., "Behavior of Shear Wall Using Various Yield Strength of Rebar, Part 1: An Experimental Study," *Proceedings of 10th International Conference on Structural Mechanics in Reactor Technology*, Anaheim, CA, H09/01, 1989, pp. 233-238.

34. Li, B., and Xiang, W., "Effective Stiffness of Squat Structural Walls," *Journal of Structural Engineering*, ASCE, V. 137, No. 12, 2011, pp. 1470-1479. doi: 10.1061/(ASCE)ST.1943-541X.0000386